Suppression of drug resistance reveals a genetic mechanism of metabolic plasticity in malaria parasites

Running title: Mechanism of malaria metabolic plasticity

Ann M. Guggisberg[1]

Philip M. Frasse[1]

Andrew J. Jezewski[1]

Natasha M. Kafai[2]

Aakash Y. Gandhi[1*]

Samuel J. Erlinger[1†]

Audrey R. Odom John[1,3#]

[1] Department of Pediatrics, Washington University School of Medicine, St. Louis, Missouri, USA

[2] Medical Scientist Training Program, Washington University School of Medicine, St. Louis, Missouri, USA

[3] Department of Molecular Microbiology, Washington University School of Medicine, St. Louis, Missouri, USA

* Current affiliation: Aakash Gandhi, Medical Scientist Training Program, UT Southwestern Medical Center, Dallas, Texas, USA

† Current affiliation: Samuel Erlinger, Medical Scientist Training Program, Johns Hopkins University, Baltimore, Maryland, USA

24 # Address correspondence to aodom@wustl.edu

ABSTRACT

In the malaria parasite *Plasmodium falciparum*, synthesis of isoprenoids from glycolytic intermediates is essential for survival. The antimalarial fosmidomycin (FSM) inhibits isoprenoid synthesis. In *P. falciparum*, we identify a loss-of-function mutation in *HAD2* (PF3D7_1226300) as necessary for FSM resistance. Enzymatic characterization reveals that HAD2, a member of the haloacid dehalogenase-like hydrolase (HAD) superfamily, is a phosphatase. Harnessing a growth defect in resistant parasites, we select for suppression of HAD2-mediated FSM resistance and uncover hypomorphic suppressor mutations in the locus encoding the glycolytic enzyme phosphofructokinase (PFK9). Metabolic profiling demonstrates that FSM resistance is achieved via increased steady-state levels of MEP pathway and glycolytic intermediates and confirms reduced PFK9 function in the suppressed strains. We identify HAD2 as a novel regulator of malaria parasite metabolism and drug sensitivity and uncover PFK9 as a novel site of genetic metabolic plasticity in the parasite. Our study informs the biological functions of an evolutionarily conserved family of metabolic regulators and reveals a previously undescribed strategy by which malaria parasites adapt to cellular metabolic dysregulation.

IMPORTANCE

Unique and essential aspects of parasite metabolism are excellent targets for development of new antimalarials. An improved understanding of parasite metabolism and drug resistance mechanisms are urgently needed. The antibiotic fosmidomycin targets the synthesis of essential isoprenoid compounds from glucose and is a

candidate for antimalarial development. Our study identifies a novel mechanism of drug resistance and further describes a family of metabolic regulators in the parasite. Using a novel forward genetic approach, we also uncover mutations that suppress drug resistance in the glycolytic enzyme PFK9. Thus, we identify an unexpected genetic mechanism of adaptation to metabolic insult that influences parasite fitness and tolerance to antimalarials.

Keywords: Plasmodium, malaria, antimalarial agents, drug resistance, metabolism, isoprenoids, fosmidomycin, suppressor, glycolysis, metabolic regulation

57 **INTRODUCTION**

58 Malaria remains a global health threat, infecting 216 million people per year and causing
59 nearly half a million deaths, mainly of pregnant women and young children (1).
60 Resistance to current therapies has limited control efforts for malaria (2, 3). New drugs
61 and a deeper understanding of drug resistance mechanisms are urgently needed.
62
63 Malaria is caused by infection with unicellular eukaryotic parasites of the genus
64 *Plasmodium*. The species *Plasmodium falciparum* is responsible for most life-
65 threatening malarial disease. As an obligate intracellular parasite of human
66 erythrocytes, *Plasmodium falciparum* has unique metabolic features that may be
67 exploited to discover new drug targets and develop new therapies. In the red blood cell
68 niche, *Plasmodium* parasites are highly dependent on glucose metabolism. Infection
69 with *Plasmodium* spp. results in a nearly 100-fold increase in glucose import in red
70 blood cells (4–6). Despite these energy requirements, the parasite demonstrates little
71 aerobic respiration via the TCA cycle. Instead, it relies on anaerobic glycolysis to
72 produce ATP (7–10).
73
74 Besides ATP production, glucose also has a number of anabolic fates in *P. falciparum*.
75 One such fate is the synthesis of isoprenoids. Isoprenoids are a large class of
76 hydrocarbons with extensive structural and functional diversity (11). In the malaria
77 parasite, isoprenoids perform several essential functions, including protein prenylation,
78 dolichylation, and synthesis of GPI anchors (12–14). Despite this diversity, all
79 isoprenoids are synthesized from a common five-carbon building block, isopentyl

80 pyrophosphate (IPP). Evolution has produced two distinct routes for IPP synthesis: the
81 mevalonate pathway, found in archaea, fungi, animals, and the cytoplasm of plants; and
82 the methylerythritol phosphate (MEP) pathway, found in most eubacteria, plant
83 chloroplasts, and apicomplexan parasites such as *P. falciparum* (15). Because it is both
84 essential for the parasite and absent from the human host, the MEP pathway is a
85 compelling target for antimalarial development. The antibiotic and antimalarial
86 fosmidomycin (FSM) is a competitive inhibitor of the first committed enzymatic step of
87 the MEP pathway, catalyzed by 1-deoxy-D-xylulose-5- phosphate reductoisomerase
88 (DXR, E.C. 1.1.1.267) (16–18). FSM has been validated as a specific inhibitor of the
89 MEP pathway in *P. falciparum* (19) and is a valuable chemical tool to study MEP
90 pathway biology and essential metabolism in the parasite. In this study, we find that
91 FSM is also a useful tool for probing glycolytic metabolism upstream of the essential
92 MEP pathway.
93
94 Parasites are likely to control the proportion of glucose used for energy production
95 versus production of secondary metabolites, such as isoprenoids. We previously used a
96 screen for FSM resistance to identify HAD1, a metabolic regulator whose loss results in
97 increased levels of MEP pathway intermediates and resistance to MEP pathway
98 inhibition. HAD1 is a cytoplasmic sugar phosphatase that dephosphorylates a number
99 of sugar phosphate intermediates upstream of the MEP pathway (20, 21). HAD1
100 belongs to the haloacid dehalogenase-like hydrolase (HAD) enzyme superfamily and
101 more specifically, the IIB and Cof-like hydrolase subfamilies (22). While HADs are found
102 in all kingdoms of life, HAD1 is most related to bacterial members of this superfamily

103 (20, 23), which have been implicated in metabolic regulation, stress response, and
104 phosphate homeostasis (24–28). However, most members of this superfamily remain
105 uncharacterized.
106
107 In this study, we describe the discovery of HAD2, a second HAD family member in *P.*
108 *falciparum*. We find that HAD2 is a cytosolic phosphatase required for metabolic
109 homeostasis. Loss of HAD2 dysregulates glycolysis and misroutes metabolites toward
110 the MEP pathway, conferring drug resistance. In our study, we harness a fitness defect
111 in *had2* parasite strains to employ an innovative screen for suppression of drug
112 resistance in the parasite. Selection for suppression of drug resistance identifies
113 mutations in *PFK9*, which encodes the canonical glycolytic regulatory enzyme,
114 phosphofructokinase. Reduction in PFK9 activity rescues the metabolic dysregulation in
115 our resistant mutants and restores FSM sensitivity. Our unique approach thus reveals
116 PFK9 as a site of exceptional metabolic plasticity in the parasite and uncovers a novel
117 genetic mechanism by which *P. falciparum* malaria parasites may adapt to metabolic
118 stress and drug selective pressure.
119
120 This article was submitted to an online preprint archive (29).
121
122
123 **RESULTS**
124 **A FSM^R strain possesses a nonsense allele of *HAD2*, homolog of the MEP**
125 **pathway regulator HAD1**

126 The MEP pathway is responsible for the synthesis of the essential isoprenoid
127 precursors isopentenyl pyrophosphate (IPP) and dimethylallyl pyrophosphate (DMAPP).
128 This pathway is specifically inhibited by the antibiotic FSM (19, 30, 31). We previously
129 generated *P. falciparum* strains resistant to FSM. Mutations in *HAD1* (PF3D7_1033400)
130 cause the resistance phenotype in a majority of these strains (20). However, the genetic
131 and biochemical basis of FSM resistance in strain E2 remained unknown. As previously
132 reported, we find that E2 is less sensitive to FSM than its wild-type 3D7 parental line
133 (Fig. 1A) (20). Strain E2 has a FSM IC_{50} of 4.8 ± 1.2 μM, significantly greater than that
134 of its parent strain (0.9 ± 0.06 μM) ($p \leq 0.01$, unpaired Student's t-test).
135
136 We find that this resistance phenotype is not due to changes in expression of the genes
137 encoding the first two, rate-limiting, steps of the MEP pathway, *DXS* and *DXR* (32–35).
138 In addition, strain E2 does not have genetic changes in the known FSM resistance locus
139 and MEP pathway regulator, *HAD1*, nor are there changes in HAD1 expression by
140 immunoblot (Figs. S1A and S1B).
141
142 To identify new genetic changes that may result in FSM resistance, we performed whole
143 genome sequencing on strain E2 and identified an A469T mutation in PF3D7_1226300
144 (PlasmoDB ID), hereafter referred to as *HAD2* (36). Variant data for strains sequenced
145 in this study can be found in Dataset S1. Sanger sequencing of the *HAD2* locus in strain
146 E2 confirmed the presence of the A469T SNP. The A469T single nucleotide
147 polymorphism (SNP) yields a truncated (R157X) protein variant and therefore we expect
148 HAD2 function is lost in strain E2. Interestingly, HAD2 is a close homolog of the known

149 MEP pathway regulator, the sugar phosphatase HAD1 (20). Sequence homology places
150 both proteins in the haloacid dehalogenase-like hydrolase (HAD) superfamily and
151 further within the IIB and Cof-like hydrolase subfamilies (Interpro IPR006379 and
152 IPR000150, respectively) (22). While no structural information exists for *P. falciparum*
153 HAD2, the structure of the *Plasmodium vivax* HAD2 (PVX_123945, PvHAD2) has been
154 solved (PDB ID 2B30). PvHAD2 (93% identical and 98% similar to PfHAD2) contains
155 the common structural motifs found in other HADs, including a core and cap domain
156 (Fig. 1B). HAD2 possesses the four conserved sequence motifs found in HAD proteins
157 (Fig. 1C), which are involved in binding of the substrate, coordination of the phosphoryl
158 group and Mg^{2+} ion, and hydrolysis of the substrate phosphate (37–39). Overall, HAD2
159 and HAD1 protein sequences share ~29% sequence identity and ~53% sequence
160 similarity (Fig. 1C). We hypothesized that HAD2, like HAD1, regulates metabolism in *P.*
161 *falciparum*, and that loss of HAD2-mediated metabolic control was responsible for FSM-
162 resistance in malaria parasite strain E2.
163
164 **HAD2 is a functional phosphometabolite phosphatase**
165 We have previously established that *P. falciparum* HAD1 is a promiscuous sugar
166 phosphatase, with activity against a wide range of phosphometabolites. Similarly, *P.*
167 *vivax* HAD2 has been enzymatically characterized and found to possess phosphatase
168 activity against various monophosphorylated substrates, including glycerol 2-phosphate
169 (glc2P) and pyridoxal phosphate (PLP) (40). Recombinant PvHAD2 also utilizes
170 additional monophosphorylated substrates, such as adenosine 5'-monophosphate
171 (AMP) and glycerol 1-phosphate (glc1P), with moderate activity.

172

173 Based on the previous characterization of a close *Plasmodium* homolog, as well as
174 sequence homology to HAD1 and other HAD proteins, we predicted that PfHAD2 would
175 also function enzymatically as a phosphatase. We successfully purified recombinant
176 PfHAD2 in *E. coli* and confirmed the phosphatase activity of recombinant PfHAD2 using
177 *para*-nitrophenyl phosphate (*p*NPP), a promiscuous, chromogenic phospho-substrate
178 (Fig. 2A) (23, 41). Because *E. coli* expresses a number of HAD-like phosphatases (23),
179 we confirmed that the phosphatase activity was specific to purified PfHAD2 by
180 expression and purification of a catalytically inactive mutant ($HAD2^{D26A}$). The Asp26
181 residue was chosen for mutagenesis as the corresponding residue in PfHAD1 (Asp27)
182 has been previously shown to be required for catalysis (21).

183

184 We also established the activity of PfHAD2 against a panel of phosphorylated
185 substrates and determined that its substrate profile closely mirrors that of PvHAD2 (Fig.
186 2B). Overall, we find that PfHAD2 is a phosphatase with activity against small
187 phosphosubstrates, such as *p*NPP and glc2P. These data suggest that, like HAD1 and
188 related HADs in microbes and plants (23, 42–44), HAD2 is a promiscuous phosphatase
189 with a preference for a variety of monophosphorylated phosphometabolites.

190

191 ***In vitro* evolution of mutations suppressing FSM resistance**

192 During routine culturing of E2 FSM^R parasites, we observed that the E2 strain is growth-
193 attenuated compared to its parental parasite strain. Surprisingly, during prolonged
194 culture in the absence of FSM, this growth phenotype resolved, and improved growth

195 rates correlated with a return to FSM sensitivity (Fig. 3A). From these observations, we
196 hypothesized that *had2*^{R157X}-mediated FSM resistance led to a fitness cost in cultured
197 parasites. We sought to harness this fitness cost to drive *in vitro* evolution of a FSM-
198 sensitive (FSM^{S}) population, possessing additional, novel mutations that might suppress
199 FSM resistance in *had2*^{R157X} parasite strains.
200
201 FSM-resistant strain E2 was cultured through multiple passages in the absence of FSM
202 selection. Through limiting dilution, we derived five E2-based clones in the absence of
203 drug pressure (Fig. 3B). Three of the five clones remained FSM^{R} (designated clones
204 E2-R1, -R2, and -R3), but two of these were found to be FSM^{S} (designated E2-S1 and -
205 S2) (Fig. 3B and 4A). To validate our novel suppressor screen approach, we
206 independently repeated this genetic selection with the three FSM^{R} E2 clones by again
207 culturing in the absence of FSM for >1 month (Fig. 3B). As before, these strains (E2-S3,
208 -S4, and -S5) also lost their FSM resistance phenotype (Fig. 4A).
209
210 Consistent with our initial observation that our *had2*^{R157X} FSM resistant strain grows
211 poorly, we find that the FSM^{R} clone E2-R1 grows at a significantly reduced rate
212 compared to the parental strain, while two FSM^{S} clones (E2-S1 and E2-S3) have
213 restored growth rates, similar to that of wild-type (Fig. 4B).
214
215 Loss of FSM resistance might have occurred by reversion of the *had2*^{R157X} mutation in
216 E2-derived strains. Instead, we find that all E2-SX clones maintained loss of HAD2 via
217 the *had2*^{R157X} mutation. We hypothesized that the FSM^{S} E2 clones, driven by a fitness

218 advantage, had acquired new suppressor mutation(s) at an additional locus. We
219 performed whole genome sequencing on the original five E2 clones to identify any
220 genetic changes that segregated with FSM-sensitivity. Sequencing revealed that a new
221 mutation (C3617T) in the locus encoding phosphofructokinase-9 (*PFK9*,
222 PF3D7_0915400) is present in both suppressed (FSM^S) E2 clones and none of the
223 three FSM^R E2 clones (Fig. 3B, Dataset S1). The C3617T mutation results in a
224 $PFK9^{T1206I}$ protein variant. *PFK9* contained the only SNP that segregated with the
225 change in FSM tolerance. Two other loci had indels that also segregated with our FSM
226 phenotype. These loci encode a tyrosine recombinase (MAL13P1.42) (45) and an
227 erythrocyte surface protein (PIESP1, PFC0435w). Given their predicted functions and
228 the presence of A/T indels in poly-A and poly-T tracts, we concluded that mutations in
229 these loci were unlikely to result in our suppressed phenotype and prioritized *PFK9* as
230 the likely locus of our suppressor mutation.
231
232 To verify whether mutations in *PFK9* were responsible for suppressing FSM resistance
233 in all of our suppressed strains, we investigated *HAD2* and *PFK9* in the E2-S3, -S4, and
234 -S5 strains, which were derived through independent evolution of the E2-R1, -R2, and -
235 R3 populations in the absence of FSM. By Sanger sequencing, we find that, as before,
236 all strains maintain the $had2^{R157X}$ mutation and acquire new, independent *PFK9*
237 mutations (Fig. 4A). The independent acquisition of four different *PFK9* alleles during
238 selection, each of which was associated with both improved growth and loss of FSM
239 sensitivity, strongly indicates that loss of PFK9 function is responsible for these
240 phenotypes in strains lacking HAD2.

241

242 **Loss of HAD2 is necessary for FSM-resistance in *had2^{R157X}* parasites**

243 HAD2 was not the sole genetic change in FSM^{R} strain E2. In addition, because
244 intraerythrocytic *P. falciparum* parasites are haploid, we cannot distinguish recessive
245 from dominant or gain-of-function mutations. Therefore, we sought to establish whether
246 restoring HAD2 expression in *trans* in a *had2^{R157X}* strain would restore FSM sensitivity.
247 Using a previously described expression system enabled by the piggyBac transposase
248 (20, 46), we expressed HAD2-GFP driven by the *heat shock protein 110* (*Hsp110*)
249 promoter (47). We confirmed that the transfected *had2^{R157X}* E2-R2 clone maintains the
250 *had2^{R157X}* allele at the endogenous locus and successfully expresses HAD2-GFP (Fig.
251 5A). Expression of HAD2-GFP in *had2^{R157X}* parasites results in restoration of FSM
252 sensitivity (Fig. 5B), confirming that loss of HAD2 is necessary for FSM resistance in
253 this strain. The resistant clone (E2-R2) has a FSM IC_{50} of 3.9 ± 0.2 μM, significantly
254 higher than that of the wild-type parent strain (0.9 ± 0.06 μM, $p \leq 0.001$, one-way ANOVA
255 and Sidak's post-test). Expression of HAD2-GFP in E2-R2 results in an IC_{50} of 0.6 ±
256 0.02 μM for FSM, significantly lower than the E2-R2 strain ($p \leq 0.001$) but not significantly
257 different than the parental strain ($p > 0.5$).

258

259 Using fluorescence microscopy, we also investigated the localization of HAD2-GFP in
260 our E2-R2 Hsp110:HAD2-GFP strain. We observe that HAD2-GFP is diffusely present
261 throughout the cytoplasm in asexual *P. falciparum* trophozoites and schizonts but
262 excluded from the digestive food vacuole (Fig. S2). This finding is consistent with the

263 lack of a predicted signal sequence for HAD2 using SignalP, PlasmoAP, and PlasMit
264 algorithms (48–50).
265
266 **PFK9 mutations in suppressed strains are hypomorphic**
267 The *PFK9* locus encodes the enzyme phosphofructokinase (PFK, E.C. 2.7.11), which
268 catalyzes the first committed and canonically rate-limiting step of glycolysis, which is the
269 conversion of fructose 6-phosphate to fructose 1,6-bisphosphate. PFK9 is comprised of
270 two domains, alpha (α) and beta (β), which are typically encoded by independent genes
271 in non-apicomplexans (51) (Fig. 6A). While in other systems the α domain is regulatory,
272 previous work on *P. falciparum* PFK9 has demonstrated catalytic activity for both
273 domains (51–55).
274
275 Of the four PFK9 variants identified in this study, three variants map to the α domain,
276 while one variant (S335L) maps to the β domain (Fig. 6A). We projected our mutations
277 on a three-dimensional model of PfPFK9 to reveal a possible structural basis for altered
278 PFK function. Three variants (S335L, T1206I, and S1267L) align and model to currently
279 available crystal structures of PFK, while a fourth allele (N1359Y) does not. While three
280 out of four mutations map to the α domain of PfPFK9 (T1206I, S1267L, N1359Y), these
281 mutations do not appear to cluster in any particular region. All mutations affect amino
282 acid residues that are physically distant from the substrate-binding pocket of either
283 domain and are not predicted to impact binding or specific catalytic residues.

284

285 Consistent with a previous study on PfPFK9 (51), attempts to purify recombinant full-
286 length PFK9 were unsuccessful. To then understand the enzymatic impacts of our
287 PFK9 variants, we quantified the native PFK specific activity in *P. falciparum* (51, 56)
288 (Fig. 6B, Fig. S3). Lysates from strains possessing *PFK9* mutations (E2-SX strains)
289 have markedly reduced specific activity of PFK compared to the parental strain (Fig.
290 6B). Combined with the diverse mutation locations (Fig. 6A), the reduced lysate PFK
291 activity in E2-SX strains suggests that a variety of genetic strategies to alter PFK
292 function can lead to resistance suppression.

293

294 **Metabolic profiling reveals mechanisms of resistance and suppression in HAD2**
295 **and PFK9 mutant parasites**

296 Reduced activity of PFK9, which catalyzes the canonical rate-limiting step in glycolysis,
297 is associated with restored FSM sensitivity to *had2* mutant strains. Therefore, we
298 anticipated that metabolic changes might underlie both resistance and suppression in
299 our E2 clones. We performed targeted metabolic profiling on the parental parasite strain
300 as well as E2 clones R1-R3 and S1-S2 (Fig. 7A, Table S1). We find that levels of the
301 MEP pathway intermediate DOXP are significantly increased in FSM^R ($had2^{R157X}$,
302 $PFK9^{WT}$) strains (Fig. 7A, $p \leq 0.05$, one-way ANOVA and Sidak's post-test). FSM is
303 competitive with DOXP for inhibition of its target enzyme DXR. Therefore, our data
304 indicate that the FSM^R strains achieve resistance via increased levels of DOXP, which
305 outcompetes FSM. We also observe a significant increase in the downstream MEP
306 metabolite, MEcPP, in our FSM^R strains ($p \leq 0.05$).

307

308 To understand the role of PFK9 in conferring and suppressing FSM resistance, we
309 determined the steady-state levels of intermediates from glycolysis, metabolites of
310 which feed into the MEP pathway (Fig. 7A, Table S1). Hierarchical clustering indicates
311 that resistant clones are characterized by a metabolic signature of increased levels of
312 FBP, DOXP, and MEcPP (Fig. 7A). We observe that the abundance of DOXP and
313 MEcPP are tightly correlated with cellular levels of the PFK9 product, FBP (Fig. 7B,
314 $p<0.01$), but not with the other upstream glycolytic metabolites, such as glu6P/fru6P
315 (Fig. 7C, $p>0.2$).

316

317 Of note, the *pfk9*^{T1206I} suppressor allele in strains S1 and S2 restores nearly parental
318 levels of FBP and downstream MEP pathway intermediates (Fig. 7A), consistent with
319 our finding that PFK activity is reduced in lysate from these strains (Fig. 6B).

320

321

322 **DISCUSSION**

323 Cells must control levels of critical metabolites in order to efficiently utilize carbon
324 sources for energy and biosynthesis of essential molecules. Cells may regulate their
325 metabolism via transcriptional, post-transcriptional, post-translational, allosteric, or
326 enzymatic mechanisms that are necessary for growth (57–60). In the glucose-rich red
327 blood cell niche, *Plasmodium* spp. malaria parasites display a unique dependence on
328 glycolysis for energy and biosynthesis.

329

330 Using resistance to a metabolic inhibitor, we identify a phosphatase member of the HAD
331 superfamily, HAD2, as a novel regulator of metabolism in *P. falciparum*. Importantly,
332 HAD2 controls substrate availability to the parasite-specific MEP pathway for isoprenoid
333 synthesis, which is a promising drug target for much needed new antimalarials. We find
334 that tolerance to inhibitors such as FSM is a robust and sensitive readout of metabolic
335 perturbation. HAD2 is necessary for metabolic homeostasis in malaria parasites. Cells
336 lacking HAD2 exhibit marked dysregulation of central carbon metabolism, including
337 altered steady-state levels of glycolytic intermediates and isoprenoid precursors. We
338 find that mutations in phosphofructokinase (*PFK9*) restore wild-type growth rates and
339 FSM sensitivity to our *had2* mutant strains. Our study thus genetically connects the
340 function of HAD2, a HAD superfamily member, to control of essential central carbon
341 metabolism. In addition, our work reveals a previously undescribed strategy by which
342 malaria parasites may respond to cellular metabolic dysregulation through mutation in
343 the gene encoding the rate-limiting glycolytic enzyme PFK9.
344
345 HAD2 is a member of the HAD superfamily and a homolog of the previously described
346 metabolic regulator HAD1. With our previous studies on HAD1 (20, 21), we define the
347 cellular role of these proteins in *P. falciparum* and contribute to the greater
348 understanding of the HADs, an evolutionarily conserved and widespread protein family.
349 Both enzymes belong to the IIB (IPR006379) and Cof-like hydrolase (IPR000150)
350 subfamilies (22). HAD enzymes display diverse substrate preferences (23, 27, 43, 44,
351 61–64), and their biological functions are largely unknown. Like other HAD homologs,
352 including PfHAD1 (20), HAD2 appears to be a non-specific, cytoplasmic phosphatase

353 with preference for small, monophosphorylated substrates. While the HAD superfamily
354 is thought to be highly evolvable pool of enzymes with broad substrate specificity (37,
355 42), our work strongly suggests that, like HAD1 and HAD2, other members of this
356 superfamily are likely to perform specific and biologically important cellular functions. As
357 *P. falciparum* has a smaller repertoire of HADs than bacteria, and *Plasmodium* HADs
358 influence easily quantified phenotypes (drug tolerance, growth, metabolite levels), the
359 malaria parasite may be an attractive system for study of the molecular mechanisms by
360 which HAD proteins control metabolic homeostasis and growth.
361
362 Metabolic profiling reveals that loss of HAD2 function leads to metabolic dysregulation,
363 which is centered around the canonical rate-limiting step of glycolysis, catalyzed by
364 PFK9. While the cellular abundance of the PFK9 product FBP is increased in *had2*
365 parasites, HAD2 does not directly utilize FBP as an enzymatic substrate, suggesting an
366 indirect mechanism of HAD2-mediated metabolic regulation. However, the distinct
367 metabolic signature of *had2* parasites, characterized by increased levels of the MEP
368 pathway metabolites DOXP and MEcPP and the key glycolytic metabolite FBP,
369 suggests that MEP pathway metabolism is precisely linked to FBP production. In other
370 microbial systems, FBP levels reflect metabolic flux and are cued to environmental
371 perturbations (65). FBP-centered metabolic regulation is also important to the related
372 apicomplexan *Toxoplasma gondii*, which constitutively expresses the fructose 1,6-
373 bisphosphatase (FBPase) to fine-tune glucose metabolism (57). While *P. falciparum*
374 does not appear to possess an FBPase, necessary for gluconeogenesis, the parasite

375 may possess alternative FBP-sensing mechanisms to tune metabolism, perhaps via
376 regulators such as HAD1 and HAD2.
377
378 The metabolic dysregulation we observe in the *had2* mutant strains appears to come
379 with a fitness disadvantage. Under FSM-selective pressure, the benefits of dysregulated
380 metabolism outweigh the costs. However, in the absence of FSM, *had2* parasites
381 achieve metabolic relief through secondary mutation in *PFK9*. The improved growth of
382 *had2 pfk9* double mutant parasites, compared to parasites with a *had2* single mutation,
383 argues that both the growth and metabolic phenotypes are linked. However, our
384 complementation studies cannot strictly discern whether restoring HAD2 directly
385 improves the growth rate of the *had2* strain, as transfection and complementation of
386 HAD2 is inherently an additional selection for increased fitness. Of note, two recent
387 essentiality screens in *Plasmodium* spp. have found that HAD2 is dispensable for
388 growth, and loss of HAD2 was not found to be associated with any significant fitness
389 defect (66, 67). However, it is unknown whether the mutant strains generated in these
390 screens have also acquired additional suppressor mutations, such as polymorphisms in
391 *PFK9*, that have facilitated their growth.
392
393 Likewise, *PFK9* provides an additional case-study of the context dependence of gene
394 essentiality in *Plasmodium* spp. As the canonical rate-limiting step in glycolysis, *PFK9* is
395 strongly predicted to be essential for asexual growth of malaria parasites (66, 67). In the
396 context of a *had2* mutation, our strains readily develop mutations in *PFK9* that reduce
397 function but are nonetheless associated with increased fitness. Indeed, it is surprising

398 that parasites that are entirely dependent on glycolysis for ATP production tolerate such
399 a significant loss of activity in this enzyme. Because we identify mutations across the
400 length of *PFK9* in our suppressed strains, our studies do not appear to point to a
401 specific disrupted function, such as alterations in an allosteric binding pocket or a dimer
402 interface. The observed mutability of *PFK9* points to a remarkable and unexpected
403 metabolic plasticity in the parasite. That is, even though the parasite inhabits a highly
404 controlled intraerythrocytic niche, a wide range of metabolic states of *P. falciparum*
405 growth are still permissive for parasite growth. This previously undescribed metabolic
406 plasticity centered on PFK9 should be considered in future efforts to target essential
407 metabolism in *Plasmodium*.
408
409 Combined with the above study, our work highlights the central role of the glycolytic
410 enzyme PFK9. A recent kinetic model of parasite glycolysis confirms that PFK has a
411 high flux-control coefficient, is sensitive to competitive inhibition, and can effectively
412 reduce glycolytic flux (68, 69). Like HAD2, PFK9 is plant-like and evolutionarily
413 divergent from its mammalian homologs (51). These differences may be exploited for
414 PFK inhibitor design and may indicate that PFK9 can be specifically targeted for
415 antimalarial development. However, our work cautions that the parasite has a surprising
416 capacity to adapt to perturbations in central carbon metabolism, which may present
417 challenges when targeting these pathways.
418
419 Finally, our approach demonstrates the power of forward genetics to uncover novel
420 biology in a clinically relevant, non-model organism. We employ a previously described

421 screen (20) to uncover a novel resistance locus and employ a second selection for
422 parasite fitness to identify changes that suppress our resistance phenotype. Of the 19
423 strains in our original FSM resistance screen (20), we identify only one *had2* mutant,
424 likely due to the reduced fitness associated with resistance in this strain. While fitness
425 costs associated with antimalarial resistance are well known (70–73), this study
426 represents, to our knowledge, the first to harness this evolutionary trade-off to identify
427 suppressor mutations in a non-target locus. Additional methods to identify low fitness
428 resistant mutants have recently been recently described (73), and fitness assessment of
429 resistance mutations may allow for suppressor screening for other antimalarials or other
430 target pathways to reveal new aspects of biology and drug resistance in malaria
431 parasites.
432
433
434 **MATERIALS AND METHODS**
435
436 **Parasite strains and culture**
437 Unless otherwise indicated, parasites were maintained at 37 °C in 5% O_2/5% CO_2/90%
438 N_2 in a 2% suspension of human erythrocytes in RPMI medium (Sigma Aldrich)
439 modified with 27 mM $NaHCO_3$, 11 mM glucose, 5 mM HEPES, 0.01 mM thymidine, 1
440 mM sodium pyruvate, 0.37 mM hypoxanthine, 10 µg/mL gentamycin, and 5 g/L Albumax
441 (Thermo Fisher Scientific).
442

443 FSM^R strain E2 was generated by selecting a clone of genome reference strain 3D7
444 (MRA-102, MR4, ATCC, Manassas, VA) under continuous treatment with 3 μM FSM, as
445 previously described (20). Clones of strain E2 were isolated by limiting dilution.
446
447 **Quantification of FSM resistance**
448 Opaque 96-well plates were seeded with asynchronous cultures at 0.5-1.0%
449 parasitemia (percent of infected red blood cells). After 3 days, media was removed and
450 parasitemia was measured via Picogreen fluorescence on a POLARStar Omega
451 spectrophotometer (BMG Labtech), as previously described (74). Half maximal
452 inhibitory concentration (IC_{50}) values were calculated using Graphpad Prism. Unless
453 otherwise indicated, all IC_{50} data are representative of means from at least ≥3
454 independent experiments performed with technical replicates.
455
456 **HAD2 structural alignment**
457 Structures were aligned using the TM-align algorithm in Lasergene Protean 3D software
458 (root mean square deviation (RMSD) of 1.9 Å).
459
460 **Whole genome sequencing and variant analysis**
461 Library preparation, sequencing, read alignment, and variant analyses were performed
462 by the Washington University Genome Technology Access Center. One microgram of
463 parasite genomic DNA was sheared, end repaired, and adapter ligated. Libraries were
464 sequenced on an Illumina HiSeq 2500 in Rapid Run mode to generate 101 bp paired
465 end reads. Reads were aligned to the *P. falciparum* 3D7 reference genome (PlasmoDB

466 v7.2) using Novoalign (V2.08.02). Duplicate reads were removed. SNPs were called
467 using samtools (quality score ≥20, read depth ≥5) and annotated using snpEff.
468 Background variants were removed using previously sequenced genomes from parental
469 and control strains (20). Mixed variant calls and variants in highly variable surface
470 antigen loci (75, 76) were removed.
471
472 **Sanger sequencing**
473 The *HAD2* (PlasmoDB PF3D7_1226300) A469T (R157X) SNP was amplified and
474 sequenced using the HAD2_R157X_F and HAD2_R157X_R primers. The *PFK9* locus
475 was amplified using the PFK9_F and PFK9_R primers. *PFK9* amplicons were
476 sequenced using the PFK9_seq (1-8) primers. Primer sequences can be found in Table
477 S2.
478
479 **Generation of recombinant HAD2**
480 The predicted coding sequence of *HAD2* was amplified using the HAD2_LIC_F and
481 HAD2_LIC_R primers (Table S2). A catalytic mutant (D26A) was also generated to use
482 as a negative control in activity assays. The $had2^{D26A}$ allele was created using the
483 HAD2_D26A_F and HAD2_D26A_R site-directed mutagenesis primers (Table S2).
484
485 Ligation-independent cloning was used to clone *HAD2* and $had2^{D26A}$ into vector BG1861
486 (77), which introduces an N-terminal 6xHis fusion to the expressed protein.
487 BG1861:6xHis-HAD2 was transformed into One Shot BL21(DE3)pLysS *Escherichia coli*
488 cells (Thermo Fisher Scientific). Protein expression was induced for 3 hours with 1 mM

489 isopropyl-β-D-thiogalactoside at mid-log phase (OD_{600} 0.4-0.5). Cells were collected by
490 centrifugation and stored at -20°C.
491
492 Cells were lysed in buffer containing 1 mg/mL lysozyme, 20 mM imidazole, 1 mM
493 dithiothreitol, 1 mM $MgCl_2$ 10 mM Tris HCl (pH 7.5), 30 U benzonase (EMD Millipore),
494 and EDTA-free protease inhibitor tablets (Roche). 6xHis-HAD2 was bound to nickel
495 agarose beads (Gold Biotechnology), washed with 20 mM imidazole, 20 mM Tris HCl
496 (pH 7.5), and 150 mM NaCl and eluted in 300 mM imidazole, 20 mM Tris HCl (pH 7.5),
497 and 150 mM NaCl. This eluate was further purified by size-exclusion gel
498 chromatography using a HiLoad 16/600 Superdex 200 pg column (GE Healthcare)
499 equilibrated in 25 mM Tris HCl (pH 7.5), 250 mM NaCl, and 1 mM $MgCl_2$. The elution
500 fractions containing HAD2 were pooled and concentrated and glycerol was added to
501 10% (w/v). Protein solutions were immediately flash frozen and stored at -80°C.
502
503 **HAD2 activity assays**
504 The rate of *para*-nitrophenyl phosphate (*p*NPP; Sigma-Aldrich S0942) hydrolysis by
505 HAD2 was determined by continuous measurement of absorbance at 405 nm. Assays
506 were performed at 37°C in 50 µl with 50 mM Tris-HCl, pH 7.5, 5 mM $MgCl_2$, 10 mM
507 *p*NPP, and 1.2 µM enzyme.
508
509 Hydrolysis of other phosphorylated substrates by HAD2 was measured using the
510 EnzChek phosphate assay kit (Life Technologies). Reaction buffer was modified to
511 contain 50 mM Tris-HCl, 1 mM $MgCl_2$, pH 7.5, 0.1 mM sodium azide, 0.2 mM 2-amino-

512 6-mercapto-7-methylpurine riboside (MESG), and 1 U/mL purine nucleoside
513 phosphorylase (PNP). Reactions contained 5 mM substrate and 730 nM enzyme.
514 Activity was normalized to that obtained from catalytically inactive 6xHis-HAD2^{D26A}. All
515 data are means from ≥3 independent experiments performed with technical replicates.
516
517 ***P. falciparum* growth assays**
518 Asynchronous cultures were seeded at 1% parasitemia. Media (no drug) was
519 exchanged daily. Samples were taken at indicated timepoints and fixed in PBS + 4%
520 paraformaldehyde, 0.05% glutaraldehyde. Cells were stained with 0.01 mg/ml acridine
521 orange and parasitemia was determined on a BD Biosciences LSRII flow cytometer
522 (Thermo Fisher Scientific). All data are means from ≥3 independent experiments.
523
524 **pTEOE110:HAD2 plasmid construction**
525 The pTEOE110 construct contains the *heat shock protein 110* (PF3D7_0708800) 5'
526 UTR and a C-terminal GFP tag (20). Human dihydrofolate reductase (hDHFR) is
527 present as a selectable marker. Inverted terminal repeats are included for genome
528 integration by a co-transfected piggyBac transposase (pHTH, MRA912, MR4, ATCC,
529 Manassas, VA).
530
531 *HAD2* was amplified with the HAD2_XhoI_F and HAD2_AvrII_R primers (Table S2) and
532 cloned into AvrII and XhoI sites in the pTEOE110 plasmid.
533
534 **Parasite transfections**

535 Transfections were performed as previously described (20). Briefly, 50-100 µg of
536 plasmid DNA was precipitated and resuspended in Cytomix (25 mM HEPES pH 7.6,
537 120 mM KCl, 0.15 mM $CaCl_2$, 2 mM EGTA, 5 mM $MgCl_2$, 10 mM K_2HPO_4).
538
539 A ring-stage *P. falciparum* culture was washed with Cytomix and resuspended in the
540 DNA/Cytomix solution. Cells were electroporated using a BioRad Gene Pulser II
541 electroporator at 950 µF and 0.31 kV. Electroporated cells were washed with media and
542 returned to normal culture conditions. Parasites expressing the construct were selected
543 by continuous treatment with 5 nM WR92210 (Jacobus Pharmaceuticals). Transfectants
544 were cloned by limiting dilution and presence of the HAD2-GFP construct was verified
545 by PCR using gene- and GFP-specific primers (HAD2_R157X_F and GFP_R, Table
546 S2). Maintenance of the endogenous *HAD2* and *PFK9* genotypes were verified by
547 Sanger sequencing.
548
549 **Antiserum generation**
550 Polyclonal anti-HAD2 antiserum was raised in rabbits against 6xHis-HAD2, with
551 Titermax as an adjuvant (Cocalico Biologicals). Antiserum specificity was confirmed by
552 immunoblot of lysate lacking HAD2. Polyclonal anti-HAD1 antiserum has been
553 previously described (MRA-1256, MR4, ATCC) (20).
554
555 **Immunoblotting**
556 Lysates were separated on a polyacrylamide gel and transferred to a polyvinylidene
557 difluoride membrane. Membranes were blocked in 5% non-fat dry milk, 0.1% Tween-20

558 in PBS. Rabbit polyclonal antisera were used at the following dilutions: 1:2,000-5,000
559 anti-HAD2 and 1:20,000 anti-HAD1 (20). For all blots, 1:20,000 HRP-conjugated goat
560 anti-rabbit IgG antibody was used as a secondary antibody (ThermoFisher 65-6120).
561 Blots were stripped with 200 mM glycine, 0.1% SDS, 1% Tween-20, pH 2.2 and re-
562 probed with 1:5,000 rabbit anti-heat shock protein 70 (Hsp70) (AS08 371, Agrisera
563 Antibodies) as a loading control. All blots shown are representative of ≥3 independent
564 experiments. Minimal adjustments were applied equally to all blot images.
565
566 **PfPFK model construction**
567 PfPFK subunits were searched against the HHpred server for protein remote homology
568 detection and 3D structure prediction using statistics as previously described (78–81).
569 The *Borellia burgdorferii* PFK structure (PDB 1KZH) (82) returned the highest similarity
570 for both PfPFK domains and was used to predict 3D structure for each domain using the
571 program MODELLER. PFK product orientation in the active site of the model was
572 predicted via the alignment tool, using PyMOL software against the *E. coli* PFK crystal
573 structure (PDB 1PFK) (83). The α domain model encompasses amino acids 779-1347
574 and the β domain model encompasses amino acids 110-638.
575
576 **Assay of native PFK9 activity**
577 Sorbitol-synchronized trophozites were isolated using 0.1% saponin. Cells were washed
578 in buffer containing 100 mM Tris-HCl (pH 7.5), 1 mM $MgCl_2$, 1 mM DTT, 10% glycerol,
579 and EDTA-free protease inhibitor tablets (Roche) and lysed by sonication at 4°C (Fisher

580 Scientific Model 550 Sonic Dismembrator, amplitude 3.5), followed by centrifugation at
581 4°C (10,000 x *g*, 10 min). An "RBC carryover" control was comprised of the trace
582 cellular material remaining after saponin lysis, centrifugation, and wash of uninfected
583 erythrocytes.
584
585 Lysate PFK9 activity was monitored by linking it to the oxidation of NADH, as previously
586 described (51, 56). Reactions contained 100 mM Tris-HCl (pH 7.5), 1 mM $MgCl_2$, 1 mM
587 DTT, 0.25 mM NADH, 1 mM ATP, 3 mM fructose 6-phosphate, and excess of linking
588 enzymes aldolase (7.5 U), triose-phosphate isomerase (3.8 U), and glycerol 3-
589 phosphate dehydrogenase (3.8 U). After adding fresh cell lysate (10-15 µg total protein),
590 absorbance at 340 nm was measured at 37°C for 40 min. Activity was determined by
591 linear regression using Graphpad Prism software. Unless otherwise indicated, data are
592 means from ≥3 independent experiments.
593
594 **Metabolite profiling**
595 Approximately ~1 x 10^9 sorbitol-synchronized early trophozites were isolated using
596 0.1% saponin, washed with ice-cold PBS + 2 g/L glucose, and frozen at -80 °C.
597 Samples were extracted in 600 µL of ice-cold extraction solvent [chloroform, methanol,
598 and acetonitrile (2:1:1, v/v/v)] using two liquid-nitrogen cooled 3.2 mm stainless steel
599 beads and homogenization in a Tissue-Lyser II instrument (Qiagen) at 20 Hz for 5
600 minutes in a cold sample rack. Ice-cold water was added and samples were
601 homogenized for 5 min at 20 Hz. Samples were centrifuged at 14,000 rcf at 4°C for 5
602 min. The polar phase was lyophilized and re-dissolved in 100 µL water and analyzed by

603 LC-MS/MS. LC-MS/MS was performed on a 4000QTRAP system (AB Sciex) in multiple-
604 reaction monitoring mode using negative ioniziation and 10 mM tributylammonium
605 acetate (pH 5.1-5.5) as the ion pair reagent. The specific parameters used for analysis
606 of MEP pathway metabolites have been previously described (19). Liquid
607 chromatography separation was performed using ion pair reverse-phase
608 chromatography (84) with the following modifications: (1) RP-hydro 100 mm × 2.0 mm,
609 2.5 µm high performance liquid chromatography column (Phenomenex), (2) flow rate of
610 0.14 mL/min, (3) solvent A of 10 mM tributylammonium acetate in 5% methanol, (4)
611 binary LC gradient (20% solvent B (100% methanol) from 0 to 2.5 min, 30% B for 12.5
612 min, 80% B for 5 min, and column equilibration at for 5 minutes), and (5) 20 µL
613 autosampler injection volume.
614
615 **Accession numbers**
616 All genome data have been deposited in the NCBI BioProject database (PRJNA222697)
617 and Sequence Read Archive (SRP038937).
618
619
620 **ACKNOWLEDGEMENTS**
621 We thank the Genome Technology Access Center in the Department of Genetics at
622 Washington University School of Medicine for help with genomic analysis. The Center is
623 partially supported by NCI Cancer Center Support Grant #P30 CA91842 to the
624 Siteman Cancer Center and by ICTS/CTSA Grant# UL1TR002345 from the National
625 Center for Research Resources (NCRR), a component of the National Institutes of

626 Health (NIH), and NIH Roadmap for Medical Research. This publication is solely
627 the responsibility of the authors and does not necessarily represent the official view
628 of NCRR or NIH. We thank Sophie Alvarez and the Proteomics and Mass Spectrometry
629 Facility at the Donald Danforth Plant Science Center for performing the LC-MS/MS
630 sample prep and analysis. This work was supported by the National Science
631 Foundation under grant number DBI-0521250 for acquisition of the QTRAP LC-MS/MS.
632 We thank Daniel Goldberg (Washington University) for supplying the pTEOE110
633 plasmid. We thank the Malaria Research Reference and Reagent Resource (MR4) for
634 providing reagents contributed by D.J. Carucci (MRA-102) and John Adams (MRA-912).
635 We thank Katherine Andrews for sharing unpublished data relevant to this study.
636
637
638 **REFERENCES**
639
640 1. World Health Organization. 2017. World Malaria Report 2017. Geneva,
641 Switzerland.
642 2. Dondorp AM, Nosten F, Yi P, Das D, Phyo AP, Tarning J, Lwin KM, Ariey F,
643 Hanpithakpong W, Lee SJ, Ringwald P, Silamut K, Imwong M, Chotivanich K, Lim
644 P, Herdman T, An SS, Yeung S, Singhasivanon P, Day NP, Lindegardh N,
645 Socheat D WN. 2009. Artemisinin resistance in *Plasmodium falciparum* malaria. N
646 Engl J Med 455–467.
647 3. Ashley EA, Dhorda M, Fairhurst RM, Amaratunga C, Lim P, Suon S, Sreng S,
648 Anderson JM, Mao S, Sam B, Sopha C, Chuor CM, Nguon C, Sovannaroth S,

649 Pukrittayakamee S, Jittamala P, Chotivanich K, Chutasmit K, Suchatsoonthorn C,
650 Runcharoen R, Hien TT, Thuy-Nhien NT, Thanh NV, Phu NH, Htut Y, Han K-T,
651 Aye KH, Mokuolu OA, Olaosebikan RR, Folaranmi OO, Mayxay M, Khanthavong
652 M, Hongvanthong B, Newton PN, Onyamboko MA, Fanello CI, Tshefu AK, Mishra
653 N, Valecha N, Phyo AP, Nosten F, Yi P, Tripura R, Borrmann S, Bashraheil M,
654 Peshu J, Faiz MA, Ghose A, Hossain MA, Samad R, Rahman MR, Hasan MM,
655 Islam A, Miotto O, Amato R, MacInnis B, Stalker J, Kwiatkowski DP, Bozdech Z,
656 Jeeyapant A, Cheah PY, Sakulthaew T, Chalk J, Intharabut B, Silamut K, Lee SJ,
657 Vihokhern B, Kunasol C, Imwong M, Tarning J, Taylor WJ, Yeung S, Woodrow
658 CJ, Flegg JA, Das D, Smith J, Venkatesan M, Plowe C V, Stepniewska K, Guerin
659 PJ, Dondorp AM, Day NP, White NJ. 2014. Spread of artemisinin resistance in
660 *Plasmodium falciparum* malaria. N Engl J Med 371:411–23.
661 4. Mehta M, Sonawat HM, Sharma S. 2006. Glycolysis in *Plasmodium falciparum*
662 results in modulation of host enzyme activities. J Vector Borne Dis 43:95–103.
663 5. Roth E. 1990. *Plasmodium falciparum* carbohydrate metabolism: a connection
664 between host cell and parasite. Blood Cells 16:453–66.
665 6. Roth EF. 1987. Malarial parasite hexokinase and hexokinase-dependent
666 glutathione reduction in the *Plasmodium falciparum*-infected human erythrocyte. J
667 Biol Chem 262:15678–82.
668 7. Bowman IB, Grant PT, Kermack WO, Ogston D. 1961. The metabolism of
669 *Plasmodium berghei*, the malaria parasite of rodents. 2. An effect of mepacrine on
670 the metabolism of glucose by the parasite separated from its host cell. Biochem J
671 78:472–8.

672 8. Krungkrai J, Burat D, Kudan S, Krungkrai S, Prapunwattana P. 1999.
673 Mitochondrial oxygen consumption in asexual and sexual blood stages of the
674 human malarial parasite, *Plasmodium falciparum*. Southeast Asian J Trop Med
675 Public Health 30:636–42.
676 9. MacRae JI, Dixon MW, Dearnley MK, Chua HH, Chambers JM, Kenny S, Bottova
677 I, Tilley L, McConville MJ. 2013. Mitochondrial metabolism of sexual and asexual
678 blood stages of the malaria parasite *Plasmodium falciparum*. BMC Biol 11:67.
679 10. Scheibel LW, Miller J. 1969. Glycolytic and cytochrome oxidase activity in
680 Plasmodia. Mil Med 134:1074–80.
681 11. Gershenzon J, Dudareva N. 2007. The function of terpene natural products in the
682 natural world. Nat Chem Biol 3:408–14.
683 12. Guggisberg AM, Amthor RE, Odom AR. 2014. Isoprenoid biosynthesis in
684 *Plasmodium falciparum*. Eukaryot Cell 13:1348–59.
685 13. Imlay L, Odom AR. 2014. Isoprenoid metabolism in apicomplexan parasites. Curr
686 Clin Microbiol Reports 1:37–50.
687 14. Jordão FM, Kimura EA, Katzin AM. 2011. Isoprenoid biosynthesis in the
688 erythrocytic stages of *Plasmodium falciparum*. Mem Inst Oswaldo Cruz 106:134–
689 141.
690 15. Lange BM, Rujan T, Martin W, Croteau R. 2000. Isoprenoid biosynthesis: the
691 evolution of two ancient and distinct pathways across genomes. Proc Natl Acad
692 Sci U S A 97:13172–7.
693 16. Koppisch AT, Fox DT, Blagg BSJ, Poulter CD. 2002. *E. coli* MEP synthase:
694 steady-state kinetic analysis and substrate binding. Biochemistry 41:236–43.

695 17. Kuzuyama T, Shimizu T, Takahashi S, Seto H. 1998. Fosmidomycin, a specific
696 inhibitor of 1-deoxy-d-xylulose 5-phosphate reductoisomerase in the
697 nonmevalonate pathway for terpenoid biosynthesis. Tetrahedron Lett 39:7913–6.
698 18. Steinbacher S, Kaiser J, Eisenreich W, Huber R, Bacher A, Rohdich F. 2003.
699 Structural basis of fosmidomycin action revealed by the complex with 2-C-methyl-
700 D-erythritol 4-phosphate synthase (IspC). Implications for the catalytic mechanism
701 and anti-malaria drug development. J Biol Chem 278:18401–7.
702 19. Zhang B, Watts KM, Hodge D, Kemp LM, Hunstad DA, Hicks LM, Odom AR.
703 2011. A second target of the antimalarial and antibacterial agent fosmidomycin
704 revealed by cellular metabolic profiling. Biochemistry 50:3570–7.
705 20. Guggisberg AM, Park J, Edwards RL, Kelly ML, Hodge DM, Tolia NH, Odom AR.
706 2014. A sugar phosphatase regulates the methylerythritol phosphate (MEP)
707 pathway in malaria parasites. Nat Commun 5:4467.
708 21. Park J, Guggisberg AM, Odom AR, Tolia NH. 2015. Cap-domain closure enables
709 diverse substrate recognition by the C2-type haloacid dehalogenase-like sugar
710 phosphatase *Plasmodium falciparum* HAD1. Acta Crystallogr D Biol Crystallogr
711 71:1824–34.
712 22. Hunter S, Jones P, Mitchell A, Apweiler R, Attwood TK, Bateman A, Bernard T,
713 Binns D, Bork P, Burge S, de Castro E, Coggill P, Corbett M, Das U, Daugherty L,
714 Duquenne L, Finn RD, Fraser M, Gough J, Haft D, Hulo N, Kahn D, Kelly E,
715 Letunic I, Lonsdale D, Lopez R, Madera M, Maslen J, McAnulla C, McDowall J,
716 McMenamin C, Mi H, Mutowo-Muellenet P, Mulder N, Natale D, Orengo C,
717 Pesseat S, Punta M, Quinn AF, Rivoire C, Sangrador-Vegas A, Selengut JD,

718 Sigrist CJA, Scheremetjew M, Tate J, Thimmajanarthanan M, Thomas PD, Wu
719 CH, Yeats C, Yong S-Y. 2012. InterPro in 2011: new developments in the family
720 and domain prediction database. Nucleic Acids Res 40:D306-12.
721 23. Kuznetsova E, Proudfoot M, Gonzalez CF, Brown G, Omelchenko M V, Borozan
722 I, Carmel L, Wolf YI, Mori H, Savchenko A V, Arrowsmith CH, Koonin E V,
723 Edwards AM, Yakunin AF. 2006. Genome-wide analysis of substrate specificities
724 of the *Escherichia coli* haloacid dehalogenase-like phosphatase family. J Biol
725 Chem 281:36149–61.
726 24. Kang MJ, Lee YM, Yoon SH, Kim JH, Ock SW, Jung KH, Shin YC, Keasling JD,
727 Kim SW. 2005. Identification of genes affecting lycopene accumulation in
728 *Escherichia coli* using a shot-gun method. Biotechnol Bioeng 91:636–42.
729 25. Kang Y, Weber KD, Qiu Y, Kiley PJ, Blattner FR. 2005. Genome-wide expression
730 analysis indicates that FNR of *Escherichia coli* K-12 regulates a large number of
731 genes of unknown function. J Bacteriol 187:1135–1160.
732 26. Pratish G, Radhakrishnan M. 2014. Engineering *Escherichia coli* for D-ribose
733 production from glucose-xylose mixtures. Ind Biotechnol 10:106–114.
734 27. Roberts A, Lee S-Y, McCullagh E, Silversmith RE, Wemmer DE. 2005. YbiV from
735 *Escherichia coli* K12 is a HAD phosphatase. Proteins 58:790–801.
736 28. Sun Y, Vanderpool CK. 2013. Physiological consequences of multiple-target
737 regulation by the small RNA SgrS in *Escherichia coli*. J Bacteriol 195:4804–15.
738 29. Guggisberg AM, Gandhi AY, Erlinger SJ, Merino EF, Cassera MB, John ARO.
739 2017. Suppressor screen connects HAD protein function to metabolic control in
740 *Plasmodium falciparum*. bioRxiv 155523.

741 30. Yeh E, DeRisi JL. 2011. Chemical rescue of malaria parasites lacking an
742 apicoplast defines organelle function in blood-stage *Plasmodium falciparum*.
743 PLoS Biol 9:e1001138.
744 31. Jomaa H, Wiesner J, Sanderbrand S, Altincicek B, Weidemeyer C, Hintz M,
745 Türbachova I, Eberl M, Zeidler J, Lichtenthaler HK, Soldati D, Beck E. 1999.
746 Inhibitors of the nonmevalonate pathway of isoprenoid biosynthesis as
747 antimalarial drugs. Science 285:1573–6.
748 32. Estévez JM, Cantero A, Reindl A, Reichler S, León P. 2001. 1-Deoxy-D-xylulose-
749 5-phosphate synthase, a limiting enzyme for plastidic isoprenoid biosynthesis in
750 plants. J Biol Chem 276:22901–9.
751 33. Mahmoud SS, Croteau RB. 2001. Metabolic engineering of essential oil yield and
752 composition in mint by altering expression of deoxyxylulose phosphate
753 reductoisomerase and menthofuran synthase. Proc Natl Acad Sci U S A 98:8915–
754 20.
755 34. Carretero-Paulet L, Cairó A, Botella-Pavía P, Besumbes O, Campos N, Boronat
756 A, Rodríguez-Concepción M. 2006. Enhanced flux through the methylerythritol 4-
757 phosphate pathway in *Arabidopsis* plants overexpressing deoxyxylulose 5-
758 phosphate reductoisomerase. Plant Mol Biol 62:683–95.
759 35. Morrone D, Lowry L, Determan MK, Hershey DM, Xu M, Peters RJ. 2010.
760 Increasing diterpene yield with a modular metabolic engineering system in *E. coli*:
761 comparison of MEV and MEP isoprenoid precursor pathway engineering. Appl
762 Microbiol Biotechnol 85:1893–1906.
763 36. Aurrecoechea C, Brestelli J, Brunk BP, Dommer J, Fischer S, Gajria B, Gao X,

764 Gingle A, Grant G, Harb OS, Heiges M, Innamorato F, Iodice J, Kissinger JC,
765 Kraemer E, Li W, Miller JA, Nayak V, Pennington C, Pinney DF, Roos DS, Ross
766 C, Stoeckert CJ, Treatman C, Wang H. 2009. PlasmoDB: a functional genomic
767 database for malaria parasites. Nucleic Acids Res 37:D539-43.
768 37. Burroughs AM, Allen KN, Dunaway-Mariano D, Aravind L. 2006. Evolutionary
769 genomics of the HAD superfamily: understanding the structural adaptations and
770 catalytic diversity in a superfamily of phosphoesterases and allied enzymes. J Mol
771 Biol 361:1003–34.
772 38. Koonin E V., Tatusov RL. 1994. Computer analysis of bacterial haloacid
773 dehalogenases defines a large superfamily of hydrolases with diverse specificity.
774 Application of an iterative approach to database search. J Mol Biol 244:125–32.
775 39. Aravind L, Galperin MY, Koonin E V. 1998. The catalytic domain of the P-type
776 ATPase has the haloacid dehalogenase fold. Trends Biochem Sci 23:127–9.
777 40. Srinivasan B, Kempaiah Nagappa L, Shukla A, Balaram H. 2015. Prediction of
778 substrate specificity and preliminary kinetic characterization of the hypothetical
779 protein PVX_123945 from *Plasmodium vivax*. Exp Parasitol 151:56–63.
780 41. Kuznetsova E, Proudfoot M, Sanders SA, Reinking J, Savchenko A, Arrowsmith
781 CH, Edwards AM, Yakunin AF. 2005. Enzyme genomics: Application of general
782 enzymatic screens to discover new enzymes. FEMS Microbiol Rev 29:263–79.
783 42. Kuznetsova E, Nocek B, Brown G, Makarova KS, Flick R, Wolf YI, Khusnutdinova
784 A, Evdokimova E, Jin K, Tan K, Hanson AD, Hasnain G, Zallot R, de Crécy-
785 Lagard V, Babu M, Savchenko A, Joachimiak A, Edwards AM, Koonin E V,
786 Yakunin AF. 2015. Functional diversity of haloacid dehalogenase superfamily

787 phosphatases from *Saccharomyces cerevisiae*: biochemical, structural, and
788 evolutionary insights. J Biol Chem 290:18678–98.
789 43. Titz B, Häuser R, Engelbrecher A, Uetz P, Alatossava T, Jutte H, Kuhn A,
790 Kellenberger E, Aravind L, Koonin EV, Baba T, Ara T, Hasegawa M, Takai Y,
791 Okumura Y, Baba M, Datsenko KA, Tomita M, Wanner BL, Mori H, Bacon DF,
792 Treffers HP, Bateman A, Coin L, Durbin R, Baykov AA, Evtushenko OA, Avaeva
793 SM, Bessman MJ, Frick DN, O'Handley SF, Cohen SS, Flaks JG, Barner HD,
794 Loeb MR, Lichtenstein J, Cox EC, Yanofsky C, Datsenko KA, Wanner BL,
795 Galperin MY, Moroz OV, Wilson KS, Murzin AG, Guzman LM, Belin D, Carson
796 MJ, Beckwith J, Harbers E, Chaudhuri NK, Heidelberger C, Herrick DJ, Major PP,
797 Kufe DW, Kamiya H, Koonin EV, Tatusov RL, Kufe DW, Major PP, Kuznetsova E,
798 Proudfoot M, Gonzalez CF, Lorkiewicz Z, Szybalski W, Lusk JE, Williams RJ,
799 Kennedy EP, Major PP, Egan E, Herrick D, Kufe DW, Maki H, Sekiguchi M,
800 Maliekal P, Vertommen D, Delpierre G, Schaftingen E Van, Nakanishi T, Sekimizu
801 K, O'Brien KP, Remm M, Sonnhammer EL, O'Donovan GA, Neuhard J, Okazaki
802 R, Kornberg A, Outten CE, O'Halloran TV, Pratt S, Shepard RL, Kandasamy RA,
803 Johnston PA, Perry W, Dantzig AH, Proudfoot M, Kuznetsova E, Brown G, Rao
804 NN, Kitagawa M, Mori H, Savchenko A, Yakunin AF, Rosner A, Yagil E, Santi DV,
805 McHenry CS, Sommer H, Thompson J, Treffers HP, Spinelli V, Belser NO,
806 Uchiyama I, Wilkinson DS, Crumley J, Zhang J, Inouye M. 2007. The *Escherichia*
807 *coli* protein YjjG is a house-cleaning nucleotidase in vivo. FEMS Microbiol Lett
808 270:49–57.
809 44. Caparrós-Martín JA, McCarthy-Suárez I, Culiáñez-Macià FA. 2013. HAD

810 hydrolase function unveiled by substrate screening: enzymatic characterization of
811 *Arabidopsis thaliana* subclass I phosphosugar phosphatase AtSgpp. Planta
812 237:943–54.
813 45. Ghorbal M, Scheidig-Benatar C, Bouizem S, Thomas C, Paisley G, Faltermeier C,
814 Liu M, Scherf A, Lopez-Rubio J-J, Gopaul DN. 2012. Initial characterization of the
815 Pf-Int recombinase from the malaria parasite *Plasmodium falciparum*. PLoS One
816 7:e46507.
817 46. Balu B, Shoue DA, Fraser MJ, Adams JH. 2005. High-efficiency transformation of
818 *Plasmodium falciparum* by the lepidopteran transposable element piggyBac. Proc
819 Natl Acad Sci U S A 102:16391–6.
820 47. Muralidharan V, Oksman A, Pal P, Lindquist S, Goldberg DE. 2012. *Plasmodium*
821 *falciparum* heat shock protein 110 stabilizes the asparagine repeat-rich parasite
822 proteome during malarial fevers. Nat Commun 3:1310.
823 48. Foth BJ, Ralph SA, Tonkin CJ, Struck NS, Fraunholz M, Roos DS, Cowman AF,
824 McFadden GI. 2003. Dissecting apicoplast targeting in the malaria parasite
825 *Plasmodium falciparum*. Science 299:705–8.
826 49. Petersen TN, Brunak S, von Heijne G, Nielsen H. 2011. SignalP 4.0:
827 discriminating signal peptides from transmembrane regions. Nat Methods 8:785–
828 6.
829 50. Zuegge J, Ralph S, Schmuker M, McFadden GI, Schneider G. 2001. Deciphering
830 apicoplast targeting signals--feature extraction from nuclear-encoded precursors
831 of *Plasmodium falciparum* apicoplast proteins. Gene 280:19–26.
832 51. Mony BM, Mehta M, Jarori GK, Sharma S. 2009. Plant-like phosphofructokinase

833 from *Plasmodium falciparum* belongs to a novel class of ATP-dependent
834 enzymes. Int J Parasitol 39:1441–53.
835 52. Bär J, Golbik R, Hübner G, Kopperschläger G. 2000. Denaturation of
836 phosphofructokinase-1 from *Saccharomyces cerevisiae* by guanidinium chloride
837 and reconstitution of the unfolded subunits to their catalytically active form.
838 Biochemistry 39:6960–8.
839 53. Kemp RG, Gunasekera D. 2002. Evolution of the allosteric ligand sites of
840 mammalian phosphofructo-1-kinase. Biochemistry 41:9426–30.
841 54. Klinder A, Kirchberger J, Edelmann A, Kopperschläger G. 1998. Assembly of
842 phosphofructokinase-1 from *Saccharomyces cerevisiae* in extracts of single-
843 deletion mutants. Yeast 14:323–34.
844 55. Theodorou ME, Cornel FA, Duff SM, Plaxton WC. 1992. Phosphate starvation-
845 inducible synthesis of the alpha-subunit of the pyrophosphate-dependent
846 phosphofructokinase in black mustard suspension cells. J Biol Chem 267:21901–
847 5.
848 56. Beutler E. 1984. Red Cell Metabolism: A Manual of Biochemical Methods. Grune
849 & Stratton, Philadelphia, PA.
850 57. Blume M, Nitzsche R, Sternberg U, Gerlic M, Masters SL, Gupta N, McConville
851 MJ. 2015. A *Toxoplasma gondii* gluconeogenic enzyme contributes to robust
852 central carbon metabolism and is essential for replication and virulence. Cell Host
853 Microbe 18:210–20.
854 58. Brown AJP, Brown GD, Netea MG, Gow NAR. 2014. Metabolism impacts upon
855 *Candida* immunogenicity and pathogenicity at multiple levels. Trends Microbiol

856 22:614–622.
857 59. Jurica MS, Mesecar A, Heath PJ, Shi W, Nowak T, Stoddard BL. 1998. The
858 allosteric regulation of pyruvate kinase by fructose-1,6-bisphosphate. Structure
859 6:195–210.
860 60. Kronstad J, Saikia S, Nielson ED, Kretschmer M, Jung W, Hu G, Geddes JMH,
861 Griffiths EJ, Choi J, Cadieux B, Caza M, Attarian R. 2012. Adaptation of
862 *Cryptococcus neoformans* to mammalian hosts: integrated regulation of
863 metabolism and virulence. Eukaryot Cell 11:109–18.
864 61. Cabello-Díaz JM, Gálvez-Valdivieso G, Caballo C, Lambert R, Quiles FA, Pineda
865 M, Piedras P. 2015. Identification and characterization of a gene encoding for a
866 nucleotidase from *Phaseolus vulgaris*. J Plant Physiol 185:44–51.
867 62. Caparrós-Martín JA, Reiland S, Köchert K, Cutanda MC, Culiáñez-Macià FA.
868 2007. *Arabidopsis thaliana* AtGppl and AtGpp2: two novel low molecular weight
869 phosphatases involved in plant glycerol metabolism. Plant Mol Biol 63:505–17.
870 63. Huang H, Pandya C, Liu C, Al-Obaidi NF, Wang M, Zheng L, Toews Keating S,
871 Aono M, Love JD, Evans B, Seidel RD, Hillerich BS, Garforth SJ, Almo SC,
872 Mariano PS, Dunaway-Mariano D, Allen KN, Farelli JD. 2015. Panoramic view of
873 a superfamily of phosphatases through substrate profiling. Proc Natl Acad Sci U S
874 A 112:E1974-83.
875 64. Liu J, Zhou W, Liu G, Yang C, Sun Y, Wu W, Cao S, Wang C, Hai G, Wang Z,
876 Bock R, Huang J, Cheng Y. 2015. The conserved endoribonuclease YbeY is
877 required for chloroplast ribosomal RNA processing in *Arabidopsis*. Plant Physiol
878 168:205–221.

879 65. Kochanowski K, Volkmer B, Gerosa L, Haverkorn van Rijsewijk BR, Schmidt A,
880 Heinemann M. 2012. Functioning of a metabolic flux sensor in *Escherichia coli*.
881 Proc Natl Acad Sci 110:1130–1135.
882 66. Bushell E, Gomes AR, Sanderson T, Anar B, Girling G, Herd C, Metcalf T,
883 Modrzynska K, Schwach F, Martin RE, Mather MW, McFadden GI, Parts L,
884 Rutledge GG, Vaidya AB, Wengelnik K, Rayner JC, Billker O. 2017. Functional
885 profiling of a *Plasmodium* genome reveals an abundance of essential genes. Cell
886 170:260–272.e8.
887 67. Zhang M, Wang C, Otto TD, Oberstaller J, Liao X, Adapa SR, Udenze K, Bronner
888 IF, Casandra D, Mayho M, Brown J, Li S, Swanson J, Rayner JC, Jiang RHY,
889 Adams JH. 2018. Uncovering the essential genes of the human malaria parasite
890 Plasmodium falciparum by saturation mutagenesis. Science 360:eaap7847.
891 68. Penkler G, du Toit F, Adams W, Rautenbach M, Palm DC, van Niekerk DD,
892 Snoep JL. 2015. Construction and validation of a detailed kinetic model of
893 glycolysis in Plasmodium falciparum. FEBS J 282:1481–511.
894 69. van Niekerk DD, Penkler GP, du Toit F, Snoep JL. 2016. Targeting glycolysis in
895 the malaria parasite *Plasmodium falciparum*. FEBS J 283:634–46.
896 70. Gabryszewski SJ, Dhingra SK, Combrinck JM, Lewis IA, Callaghan PS, Hassett
897 MR, Siriwardana A, Henrich PP, Lee AH, Gnädig NF, Musset L, Llinás M, Egan
898 TJ, Roepe PD, Fidock DA. 2016. Evolution of fitness cost-neutral mutant PfCRT
899 conferring *P. falciparum* 4-aminoquinoline drug resistance is accompanied by
900 altered parasite metabolism and digestive vacuole physiology. PLOS Pathog
901 12:e1005976.

902 71. Hastings IM, Donnelly MJ. 2005. The impact of antimalarial drug resistance
903 mutations on parasite fitness, and its implications for the evolution of resistance.
904 Drug Resist Updat 8:43–50.
905 72. Rosenthal PJ. 2013. The interplay between drug resistance and fitness in malaria
906 parasites. Mol Microbiol 89:1025–1038.
907 73. Lim MY-X, LaMonte G, Lee MCS, Reimer C, Tan BH, Corey V, Tjahjadi BF, Chua
908 A, Nachon M, Wintjens R, Gedeck P, Malleret B, Renia L, Bonamy GMC, Ho PC-
909 L, Yeung BKS, Chow ED, Lim L, Fidock DA, Diagana TT, Winzeler EA, Bifani P.
910 2016. UDP-galactose and acetyl-CoA transporters as *Plasmodium* multidrug
911 resistance genes. Nat Microbiol 1:16166.
912 74. Corbett Y, Herrera L, Gonzalez J, Cubilla L, Capson TL, Coley PD, Kursar TA,
913 Romero LI, Ortega-Barria E. 2004. A novel DNA-based microfluorimetric method
914 to evaluate antimalarial drug activity. Am J Trop Med Hyg 70:119–24.
915 75. Su XZ, Heatwole VM, Wertheimer SP, Guinet F, Herrfeldt JA, Peterson DS,
916 Ravetch JA, Wellems TE. 1995. The large diverse gene family var encodes
917 proteins involved in cytoadherence and antigenic variation of *Plasmodium*
918 *falciparum*-infected erythrocytes. Cell 82:89–100.
919 76. Kyes SA. 1999. Rifins: A second family of clonally variant proteins expressed on
920 the surface of red cells infected with *Plasmodium falciparum*. Proc Natl Acad Sci
921 U S A 96:9333–9338.
922 77. Alexandrov A, Vignali M, LaCount DJ, Quartley E, de Vries C, De Rosa D,
923 Babulski J, Mitchell SF, Schoenfeld LW, Fields S, Hol WG, Dumont ME, Phizicky
924 EM, Grayhack EJ. 2004. A facile method for high-throughput co-expression of

925 protein pairs. Mol Cell Proteomics 3:934–8.
926 78. Zimmermann L, Stephens A, Nam S-Z, Rau D, Kübler J, Lozajic M, Gabler F,
927 Söding J, Lupas AN, Alva V. 2017. A completely reimplemented MPI
928 bioinformatics toolkit with a new HHpred server at its core. J Mol Biol.
929 79. Söding J. 2005. Protein homology detection by HMM-HMM comparison.
930 Bioinformatics 21:951–60.
931 80. Hildebrand A, Remmert M, Biegert A, Söding J. 2009. Fast and accurate
932 automatic structure prediction with HHpred. Proteins 77 Suppl 9:128–32.
933 81. Meier A, Söding J. 2015. Automatic prediction of protein 3D structures by
934 probabilistic multi-template homology modeling. PLoS Comput Biol 11:e1004343.
935 82. Moore SA, Ronimus RS, Roberson RS, Morgan HW. 2002. The structure of a
936 pyrophosphate-dependent phosphofructokinase from the Lyme disease
937 spirochete *Borrelia burgdorferi*. Structure 10:659–671.
938 83. Shirakihara Y, Evans PR. 1988. Crystal structure of the complex of
939 phosphofructokinase from *Escherichia coli* with its reaction products. J Mol Biol
940 204:973–94.
941 84. Luo B, Groenke K, Takors R, Wandrey C, Oldiges M. 2007. Simultaneous
942 determination of multiple intracellular metabolites in glycolysis, pentose
943 phosphate pathway and tricarboxylic acid cycle by liquid chromatography-mass
944 spectrometry. J Chromatogr 1147:153–64.
945

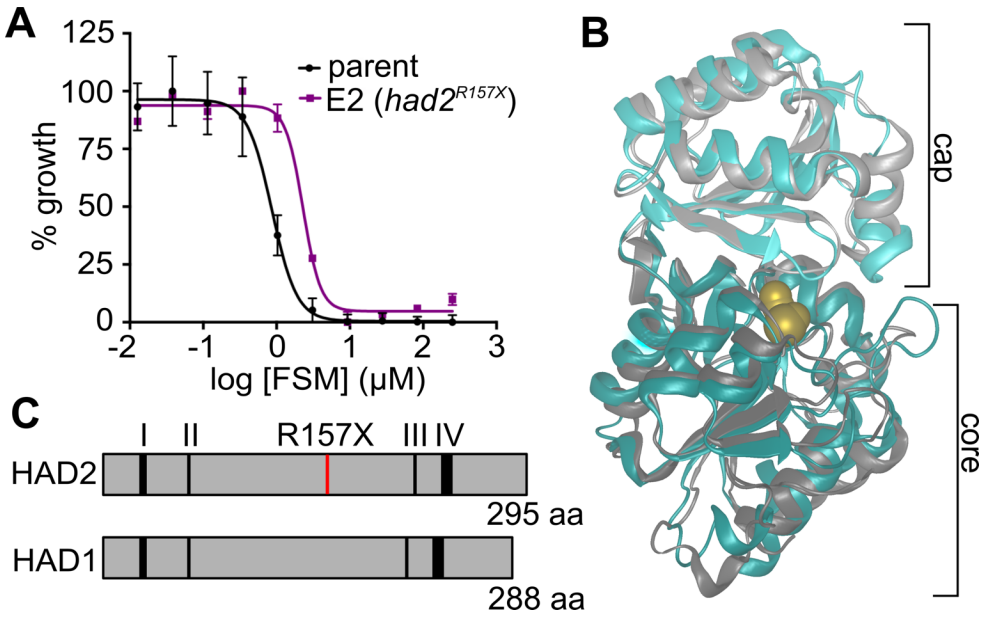

946

947 **Figure 1. FSM^R strain E2 possesses a mutation in HAD2, a homolog of the MEP**

948 **pathway regulator HAD1. (A)** Representative FSM dose-response of the parental

949 strain and strain E2. **(B)** *P. vivax* HAD2 (teal, PDB 2B30) is structurally similar to

950 PfHAD1 (grey, PDB 4QJB). Ions (Mg^{2+}, Ca^{2+}, Cl^-) are shown in yellow. **(C)** HAD2 is a

951 homolog of HAD1 (29% identity and 53% similarity) and possesses all conserved HAD

952 sequence motifs required for catalysis (37).

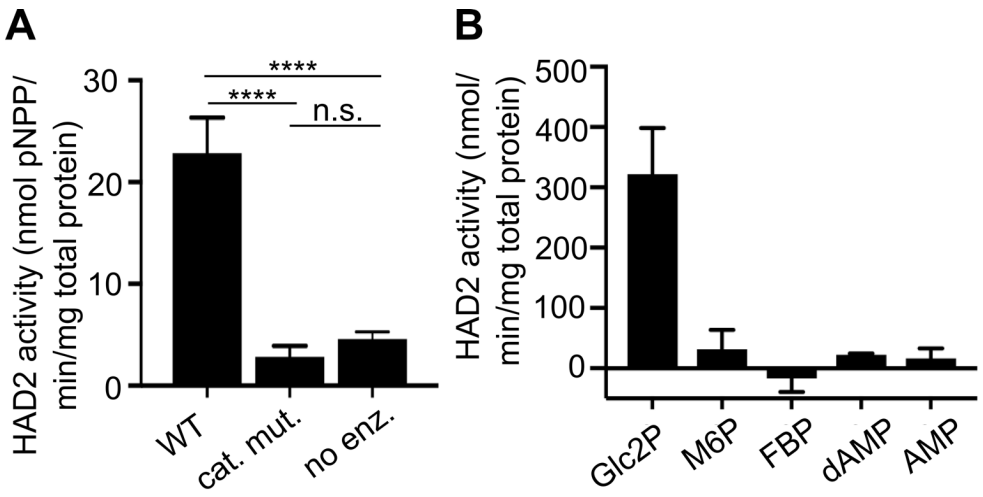

953

954 **Figure 2. PfHAD2 is a phosphatase. (A)** HAD2 is an active phosphatase, and
955 HAD2^{D26A} is a catalytic mutant (cat. mut.) that can be used as a negative control for
956 HAD2 specific activity. “No enz” represents a no enzyme control. Data shown are the
957 enzyme activities using the synthetic phosphatase substrate *p*NPP. Error bars represent
958 S.E.M. (**** = p≤0.0001, unpaired t-test). **(B)** Activity of HAD2, normalized to the activity
959 of the catalytic mutant (HAD2^{D26A}), for variety of substrates (2-GlcP, 2-glycerol-
960 phosphate; M6P, mannose-6-phosphate; FBP, fructose-2,6-bisphosphate; dAMP,
961 deoxy-adenosine monophosphate; AMP, adenosine monophosphate). Error bars
962 represent S.E.M.

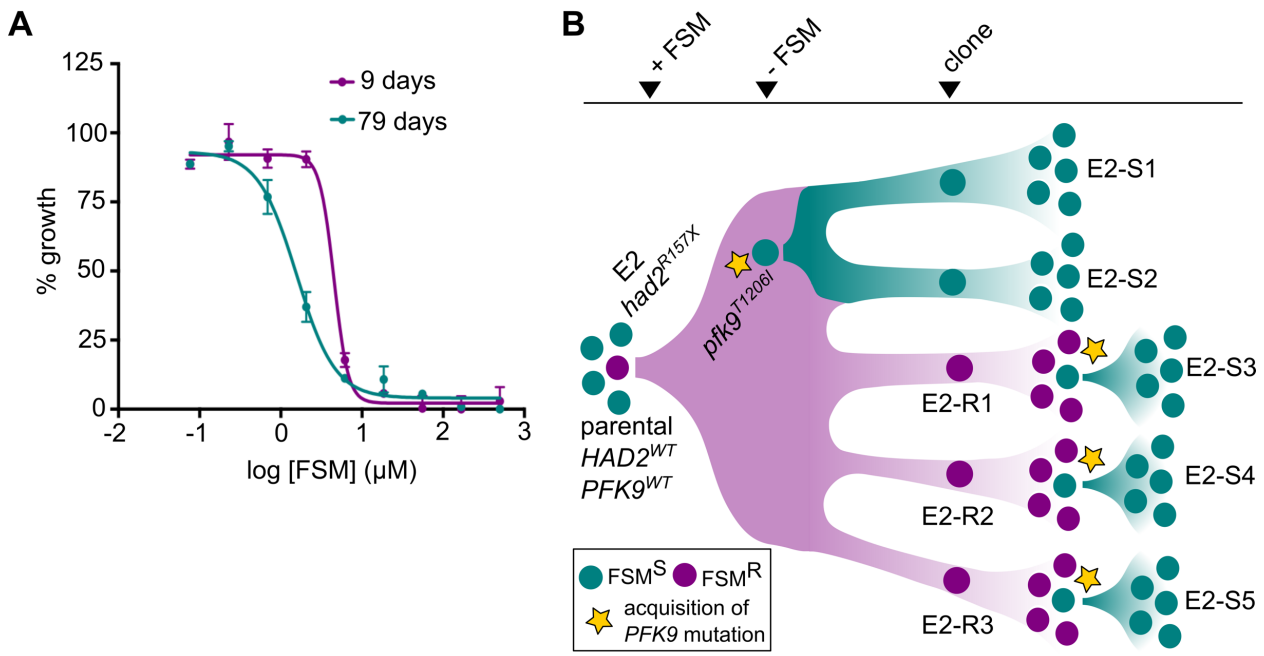

963

964 **Figure 3. Leveraging a resistance-associated growth attenuation to identify**

965 **genetic changes that modulate FSM sensitivity.**

966 **(A)** Prolonged culture results in loss of FSM resistance in strain E2. Shown are single

967 FSM dose-responses of the strain E2 before (9 days) and after (79 days) prolonged

968 culture without FSM. Nine days after thawing the resistant E2, we observe a FSM IC_{50}

969 of 4.9 μM, while after 79 days of culture without FSM, E2 has an IC_{50} of 1.3 μM. Each

970 data point is representative of the mean from two technical replicates. Error bars

971 represent S.E.M. **(B)** Parasites are colored by their FSM phenotype (teal, FSM^S; purple,

972 FSM^R). Cloned strains are named by FSM phenotype (E2-SX, sensitive; E2-RX,

973 resistant). A FSM^S parental strain was selected under FSM pressure to enrich for FSM^R

974 strain E2 (*had2*^{R157X}). After relief of FSM pressure, a fitness advantage selects for

975 spontaneous suppressor mutations in *PFK9* (*pfk9*^{mut}, yellow star) that result in FSM

976 sensitivity. FSM^R clones are grown without FSM pressure and a fitness advantage

977 again selects for suppressor mutations in *PFK9* that result in increased growth rate and

978 loss of FSM resistance.

979

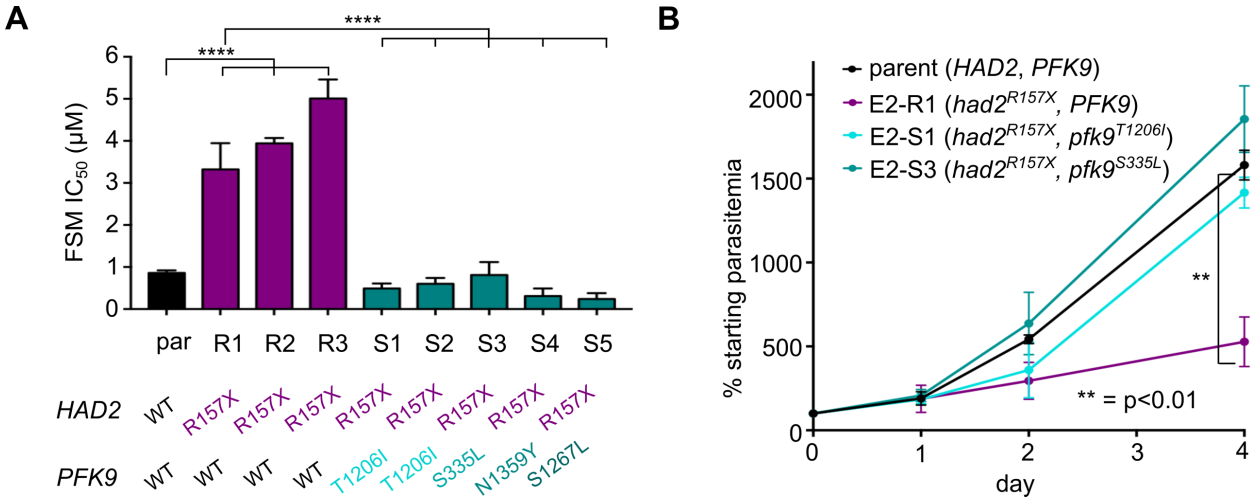

980

981 **Figure 4. Suppressor strains with *PFK9* mutations display changes in FSM**

982 **tolerance and growth.**

983 **(A)** Suppressed clones have significantly lower FSM IC_{50}s (**** = p≤0.0001). Error bars

984 represent S.E.M. *HAD2* and *PFK9* genotypes for each strain are indicated. **(B)** FSM

985 resistance results in a fitness cost. A representative FSM^R clone with the $had2^{R157X}$

986 allele (R1, purple line) has a reduced growth rate compared to the wild-type parental

987 strain (black) (** = p≤0.01). The growth defect is rescued in two representative clones

988 with mutations in *PFK9* (S1 and S3, teal lines). Growth is normalized to parasitemia on

989 day 0. Error bars represent S.E.M. from independent growth experiments.

990

991

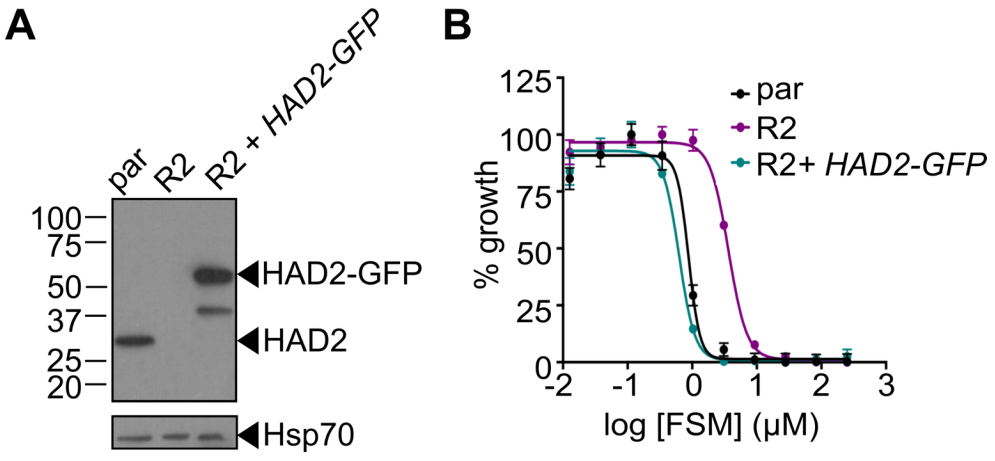

992

993

994 **Figure 5. Loss of HAD2 is necessary for FSM resistance. (A)** Successful expression

995 of pTEOE110:HAD2-GFP in strain R2 (*had2*^{R157X}, *PFK9*) was confirmed by immunoblot.

996 Marker units are kilodaltons (kDa). The top blot was probed with anti-HAD2 antiserum

997 (expected masses: HAD, 33 kDa; HAD2-GFP, 60 kDa). The bottom blot was probed

998 with anti-heat shock protein 70 (Hsp70) antiserum as a loading control. **(B)**

999 Representative FSM dose-response demonstrating expression of HAD2-GFP in strain

1000 R2 (*had2*^{R157X}, *PFK9*) results in restored sensitivity to FSM. Strain R2 has an elevated

1001 FSM IC_{50} compared to the parental strain. When HAD2 expression is restored in strain

1002 R2, the resulting strain has an IC_{50} near that of the parent strain.

1003

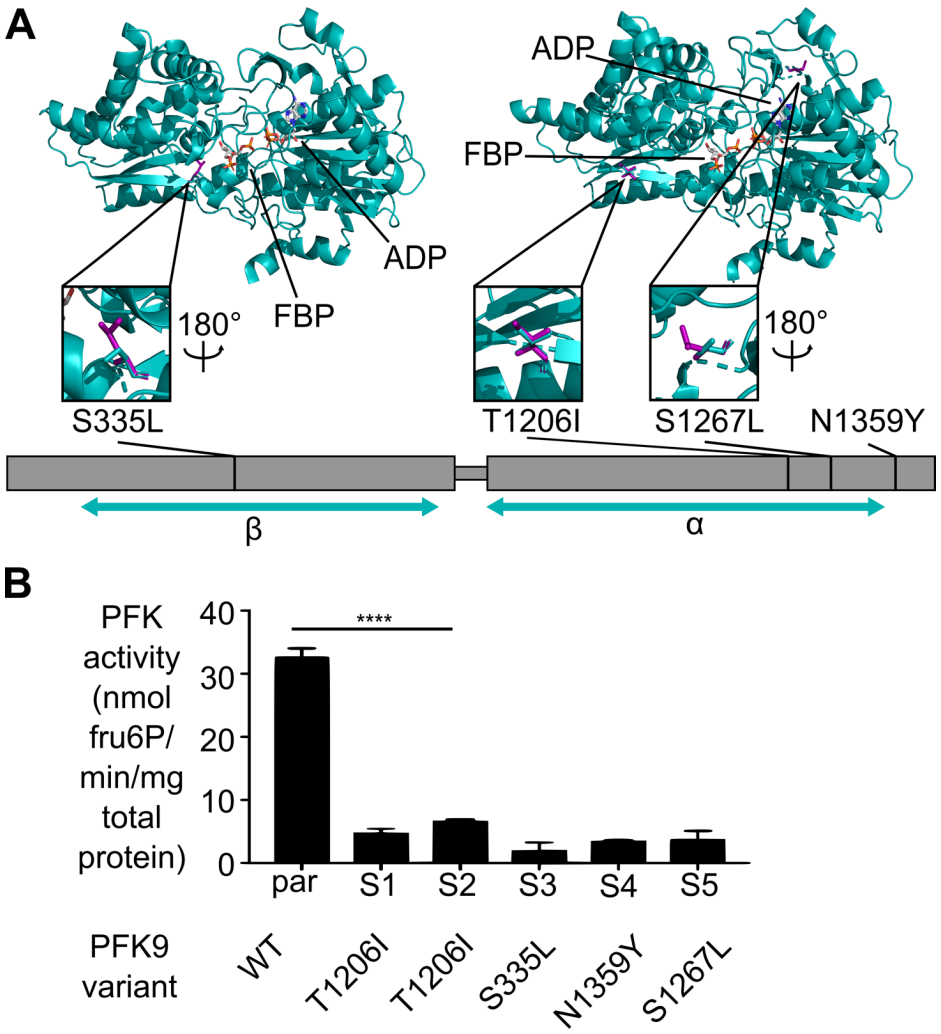

1004

1005

1006 **Figure 6. *PFK9* alleles in suppressed strains are hypomorphic. (A)** Schematic of

1007 suppressor mutations found in *PFK9*. Resulting amino acid changes and strain names

1008 are indicated. Three of the four mutations are found on the structural model of

1009 PfPFK. The parts of the protein represented by the model are notated by the teal arrows

1010 under the α and β domains. Total protein length is 1418 amino acids. N1359Y fits

1011 outside of the model. The other mutations are represented by their stick model structure

1012 with the resulting change shown in magenta. Orientations of the close-up

1013 representations of the mutations are indicated when they differ from the main model. **(B)**

1014 Measurement of PFK activity of *P. falciparum* lysate indicates that E2-SX clones with
1015 *PFK9* suppressor mutations have significantly reduced PFK activity (**** = $p \leq 0.0001$,
1016 ANOVA, Sidak's post-test). Error bars represent S.E.M. Assay is linear with respect to
1017 protein content and specific for PfPFK9 activity (S3 Fig).
1018

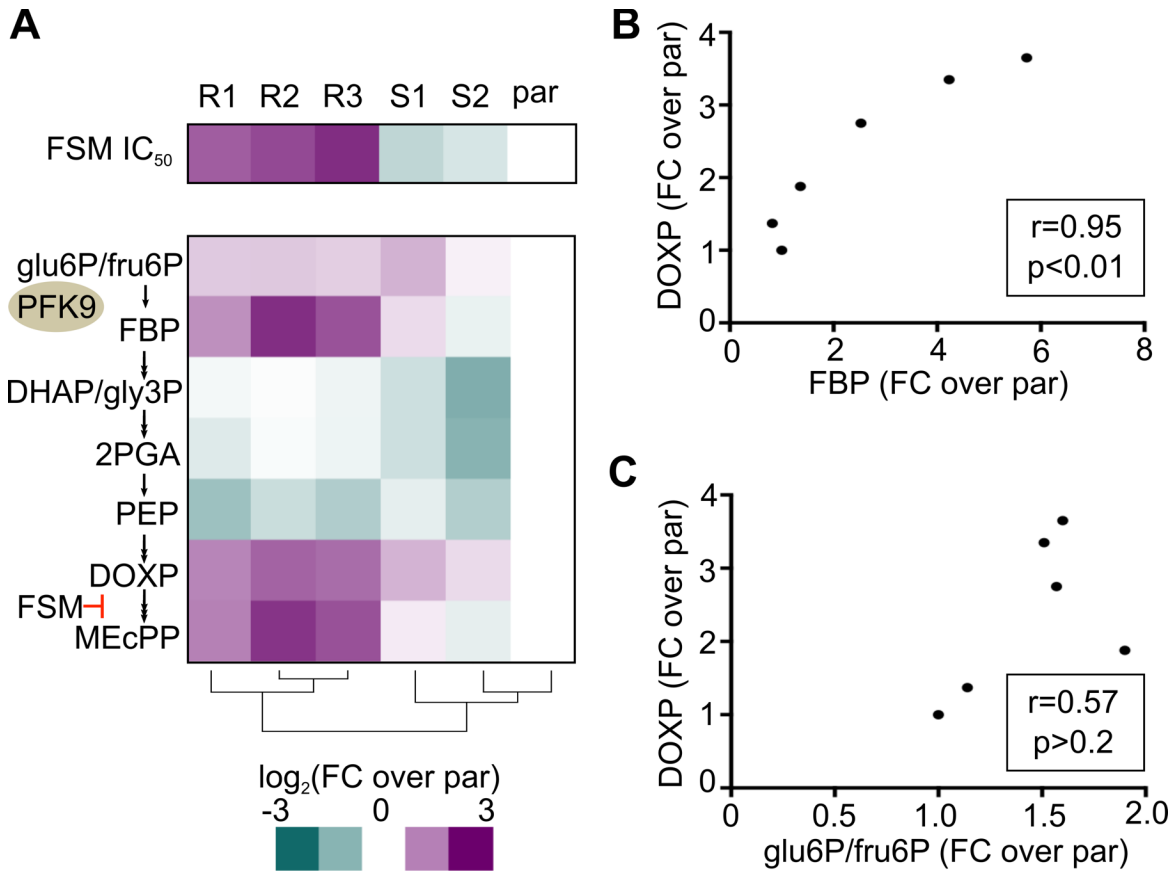

Figure 7. *HAD2* and *PFK9* alleles alter FSM resistance and metabolite levels in *P. falciparum*. (A) Metabolic profiling and clustering of parental and E2 clone strains demonstrates a metabolic signature of resistance, which includes increased levels of MEP pathway intermediates DOXP and MEcPP and the glycolytic metabolite and PFK product FBP. Glu6P/fru6P and DHAP/gly3P are isomer pairs that cannot be confidently distinguished. Clustering performed using the heatmap function in R. Data are also summarized in S1 Table. FSM IC_{50}s are shown for reference**. (B)** DOXP levels are highly correlated to levels of the upstream glycolytic metabolic FBP (Pearson's r=0.95). **(C)** In contrast, DOXP levels are not correlated to the glycolytic metabolites glu6P/fru6P (Pearson's r=0.57).

1031 **SUPPLEMENTAL MATERIAL LEGENDS**

1032

1033 **Supplemental Figure 1. FSM^R strain E2 does not have increased expression of**

1034 ***DXS*, *DXR*, or *HAD1*.**

1035 **Supplemental Figure 2. HAD2 is cytosolic.**

1036 **Supplemental Figure 3. Assay of PFK activity from *P. falciparum* lysate is linear**

1037 **and specific.**

1038 **Supplemental Table 1. Relative metabolite levels in strains described in this**

1039 **study.**

1040 **Supplementary Table 2. Primers used in this study.**